6
Orographic Effects

http://www.staff.science.uu.nl/~delde102/AtmosphericDynamics.htm

The role of the forecaster in the era of automated numerical weather prediction

In spite of progress in the development of quantitative techniques, the conventional forecaster will have an important part to play. His wide experience of local and regional conditions, orographic and topographic influences, moisture and pollution sources, etc., will be invaluable in supplementing the machine-made forecasts. While the machines provide the answers that can be computed routinely, the forecaster will have the opportunity to concentrate on the problems, which can be solved only by resort to scientific insight and experience. Furthermore, since the machine-made forecasts are derived, at least in part, from idealized models, there will always be an *unexplained residual*, which invites study. It is important, therefore, that the forecaster be conversant with underlying theories, assumptions, and models.
Sverre Petterssen (1956), **Weather Analysis and Forecasting**, volume 1, p. vii-viii.

6.1 Flow over mountains: Froude number

The "unexplained residual, which invites study", referred to by Sverre Pettersen in 1956 (quoted above), is frequently associated with effects due to the interaction of the atmosphere with mountains, valleys and coast lines. This interaction produces weather phenomena such as stationary lee buoyancy waves, downslope windstorms, "föhn", lee vortices, vortex streets, katabatic winds and the sea/land breeze. An example of a lee vortex is shown in **figure 1.4**.

Horizontal dimensions of mountain ranges are typically in the order of $L \approx 100$-1000 kilometres. An air-parcel, travelling at a typical speed, u_0, of about 10 m s^{-1} in the troposphere, takes $L/u_0 \approx 3$-30 hours to cross a mountain range with these dimensions. The response of the atmospheric flow pattern in the vicinity of the mountain depends on the imposed timescale, L/u_0, of the disturbance (or forcing) relative to the time-scales associated with the natural periods of response of the atmosphere, i.e. the period associated with

buoyancy waves, $2\pi/N$ (eq. 1.72), and with inertial waves, $2\pi/F$ (eq. 1.96). If u_0, N and F are constant, we can distinguish several regimes:

(i) **Potential flow regime** ($L/u_0<2\pi/N$). In this case the atmosphere is forced at a frequency exceeding the cut-off frequency, N (chapter 3). The reaction of the atmosphere is basically "evanescent" (section 3.3), i.e. the air-parcels follow the topography exactly, while the amplitude of the vertical displacements decays with height.

(ii) **Wave regime** (L/u_0 is not much greater than $2\pi/N$ and significantly smaller than $2\pi/F$). If the atmosphere is forced with a frequency approaching N, buoyancy waves are generated in which air-parcels oscillate nearly vertically. For lower frequencies ($<N$) air-parcels are set into a more oblique buoyancy oscillation in which effects due to the Coriolis force become increasingly important as the frequency approaches F. An indication of the existence of (stationary) buoyancy oscillations excited by mountains is given in **figure 6.1**.

(iii) **Balanced flow regime** (L/u_0 is of the same order of magnitude as, or greater than, $2\pi/F$). The frequency of forcing lies outside the range of possible free buoyancy-inertia oscillations. Rossby waves (section 1.37) are generated instead. "Potential vorticity dynamics" is important in this regime.

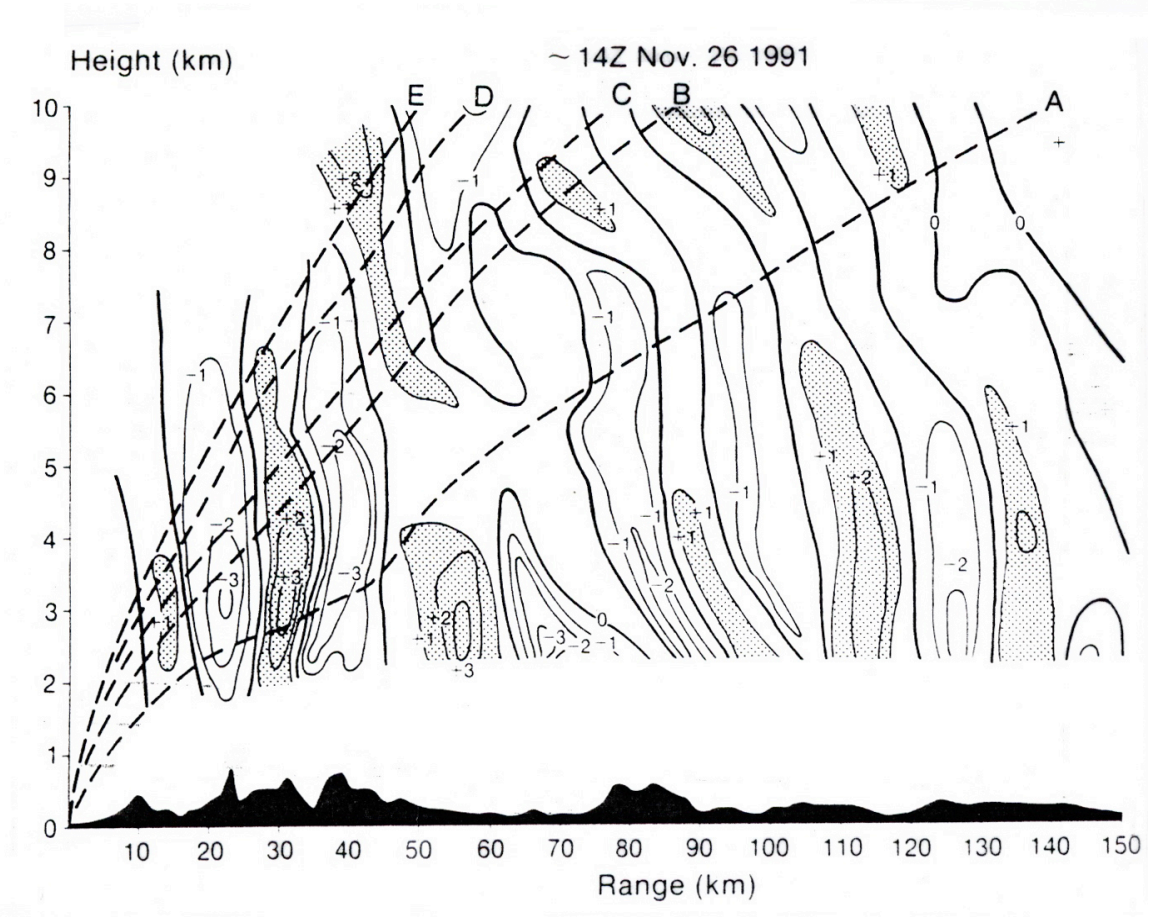

FIGURE 6.1. The vertical velocity associated with mountain generated trapped buoyancy waves. This is a subjective analysis of the vertical velocity in the vertical plane oriented along a bearing of 042 degrees and passing through Eskmeals (Lake district, England). The analysis is based on the measurements made with five sondes. The dashed lines show the paths of the five sondes and the shading indicates regions where $w>1$ m s^{-1}. The dominant horizontal wavelength is approximately 20 km and the amplitude of the wave has a maximum at a height of about 3 km, with vertical velocities of up to 3.5 m s^{-1}. Above 5 km the wave amplitude becomes small and the phase lines have an upstream tilt with height. (from G.Shutts and A.Broad, 1993: A case study of lee waves over the Lake District in northern England. **Q.J.R.Meteorol.Soc**, 119, 377-408).

The first two cases can be defined also in terms of a **Froude number**, Fr, defined as

$$Fr = \frac{2\pi u_0}{LN} \ . \tag{6.1}$$

The evanescent regime corresponds to $Fr>1$, while the wave regime corresponds to $Fr\leq 1$. At larger time-scales the influence of the Earth's rotation becomes increasingly important. Therefore, the inertial frequency becomes the relevant time-scale instead of the Brunt-Väisälä frequency. Thus, the latter regime can be defined in terms of a **Rossby number**,

$$Ro = \frac{2\pi u_0}{LF} \ . \tag{6.2}$$

Regime (iii) is characterized by Ro of order 1 or less.

6.2 Stationary and transient response

The basis of present-day theories on mountain waves was layed in the 1940's and 1950's, principally by Queney, Scorer and Long[171]. The approach of the former two authors, however, was quite different from that of the latter author. Queney and Scorer tackled the problem by applying the linear theory of a continuously stratified fluid. In contrast, Long used the shallow water equations (chapter 5).

There is, however, one point of resemblance. All three authors were concerned almost exclusively with the "stationary" or "steady" response of the air-flow to forcing by mountains. They neglected the "transient" response. The term "stationary" means that local time-derivatives are zero. For waves this implies that the horizontal phase velocity, c_x, is zero, therefore that waves-crests do not propagate.

The difference between the transient and the stationary response as well as several other typical effects of mountains on fluid flow can be illustrated with the help of the **one-layer "hydraulic" model**, described in section 5.2, assuming that $h_s\neq 0$ and retaining for the moment the derivatives with respect to y. In fact, we assume that h_s depends only on the x-coordinate. The governing equations are

$$\frac{du}{dt} = -g\frac{\partial}{\partial x}\left(h + h_s\right) + fv \ , \tag{6.3a}$$

$$\frac{dv}{dt} = -g\frac{\partial h}{\partial y} - fu \tag{6.3b}$$

$$\frac{dh}{dt} = -h\left(\frac{\partial u}{\partial x} + \frac{\partial v}{\partial y}\right) \ . \tag{6.3c}$$

Let us assume that f is constant and that

---

[171]Queney, P., 1948: The problem of air-flow over mountains. A summary of theoretical results. **Bull.Amer.Meteorol.Soc**., 29, 16-25.

Scorer, R.S., 1949: Theory of waves in the lee of mountains. **Q.J.R.Meteorol.Soc.**, 75, 41-56.

Long, R.R., 1953: Some aspects of the flow of stratified fluids. I A theoretical investigation. **Tellus**, 5, 42-57.

$$h = H(y) + h'(x,t) \tag{6.4a}$$

and

$$u = u_g + u'(x,t)\ ,\ v = v'(x,t), \tag{6.4b}$$

where the time-independent state conforms to geostrophic balance, i.e.

$$g\frac{\partial H}{\partial y} = -fu_g\ . \tag{6.5}$$

In other words, as in section 5.5, we assume the existence of a time-independent meridional geopotential gradient, which is maintained by external forcing. The associated pressure gradient force is in balance with Coriolis force associated with a time-independent zonal geostrophic flow, u_g.

The equations governing the dynamics of the "shallow water" layer flowing over the orography are (eq. 6.3a-c)

$$\frac{\partial u}{\partial t} + u\frac{\partial u}{\partial x} = -g\frac{\partial}{\partial x}(h + h_s) + fv\ , \tag{6.6a}$$

$$\frac{\partial v}{\partial t} + u\frac{\partial v}{\partial x} = -f(u - u_g)\ , \tag{6.6b}$$

$$\frac{\partial h}{\partial t} = -\frac{\partial hu}{\partial x} - v\frac{\partial H}{\partial y}. \tag{6.6c}$$

Let us place a **bell-shaped mountain with a maximum height**, H_b, at x=3000 km. Starting with a mean geostrophic flow velocity, u_g, and a free surface that is horizontal in the x-direction (but with a constant negative slope in the y-direction!), we can integrate eqs (6.6a-c) numerically to find out what happens afterwards. The result is shown in **figure 6.2**. The flow is partly **blocked** by the mountain. As a result of this fact, transient gravity-inertia waves are excited, which propagate in opposite directions away from the mountain. Initially, the wave propagating downstream is a wave of depression, whereas the wave propagating upstream is a wave of elevation. After 48 hours, however, this qualification does not hold anymore, due to dispersion caused by the Coriolis-effect. The upstream gravity-inertia wave leaves behind a region with lower flow-velocities and higher free-surface elevations. Thus, a horizontal pressure gradient is set up with high-pressure upstream and low-pressure downstream from the mountain. Due to this pressure gradient, the fluid is accelerated ($\partial u/\partial x$>0) up the mountain. This acceleration (or divergence) induces a negative meridional (y-) component in the flow through the Coriolis-effect and also a negative relative vorticity upstream of the mountain crest. In the lee of the mountain the fluid is decelerated ($\partial u/\partial x$<0) with the opposite effect on the relative vorticity, i.e. a “lee-trough” or “lee-cyclone” is formed.

It is somewhat counter-intuitive to observe that there is **mass-divergence upstream of the mountain** crest and mass-convergence downstream of the mountain crest. Nevertheless, this fact can be easily deduced from the governing equations (eqs. 6.6a-c). If we assume a stationary state (local time derivatives equal to zero) in the vicinity of the mountain, we can derive an equation for the divergence (du/dx). By eliminating $\partial h/\partial x$ from (6.6a) and (6.6c), we obtain the following expression for the divergence or acceleration.

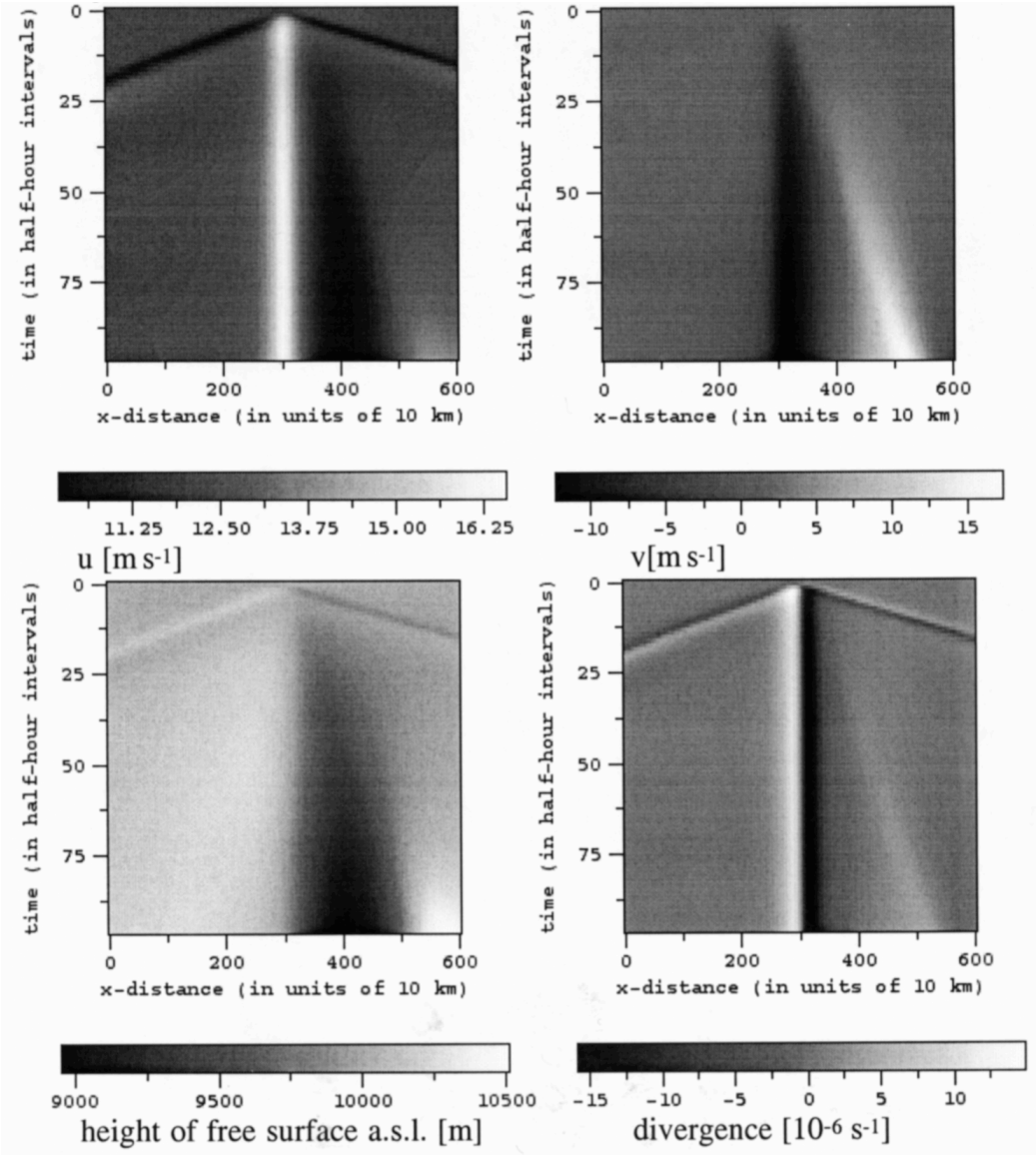

FIGURE 6.2a. Hovmöller diagrams displaying the evolution in time of the *x*-component and *y*-component of the flow velocity, height of the free surface above "sea level" and the divergence in a numerical integration of eqs. 6.3a-c (the one-layer "hydraulic" model) starting with a horizontal free surface everywhere, a constant geostrophic velocity, u_g = 12 m s^{-1}, and a bell-shaped mountain with a maximum height, H_b, of 3000 m in the middle of the domain. The mountain profile is shown in **figure 6.2b**. The fluid depth far from the mountain is 10000 m. The values of other parameters are g=1 m s^{-2} and f=0.0001 s^{-1}. The magnitude of the Froude number (see eq. 6.8) far upstream is 0.126, while over the mountain crest it reaches a maximum value of 0.212.

$$\frac{du}{dx} = \frac{u}{h\left(1 - Fr^2\right)}\left(\frac{dh_s}{dx} - \frac{fv}{g}\left(1 - \frac{u_g}{u}\right)\right) . \qquad (6.7)$$

The **Froude number**, *Fr*, in the context of this model is defined as,

$$Fr \equiv \frac{u}{\sqrt{gh}} . \qquad (6.8)$$

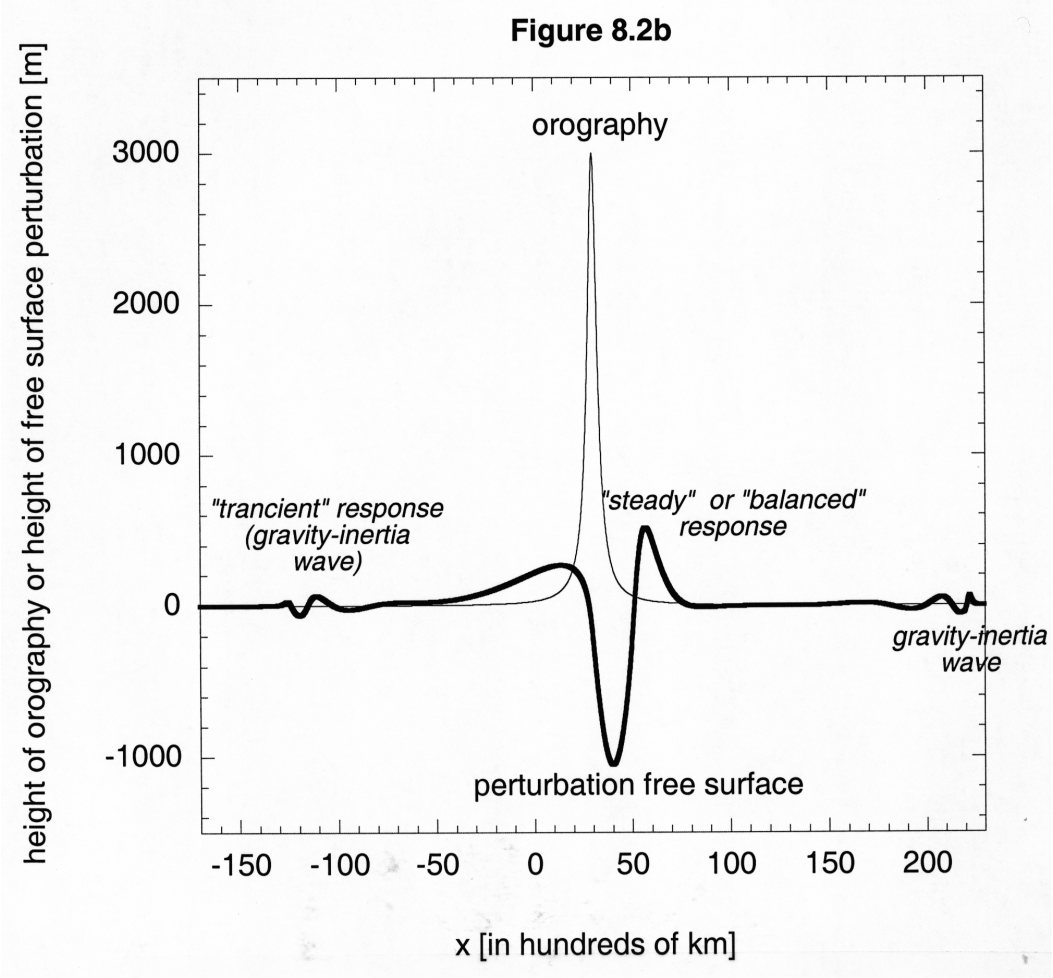

FIGURE 6.2b. Height of the earth's surface "above sea level" and perturbation of the height of the free surface at t=48 hours as a function of x. The mountain crest is located at x=3000 km. For the values of the other parameters, see **figure 6.2a**.

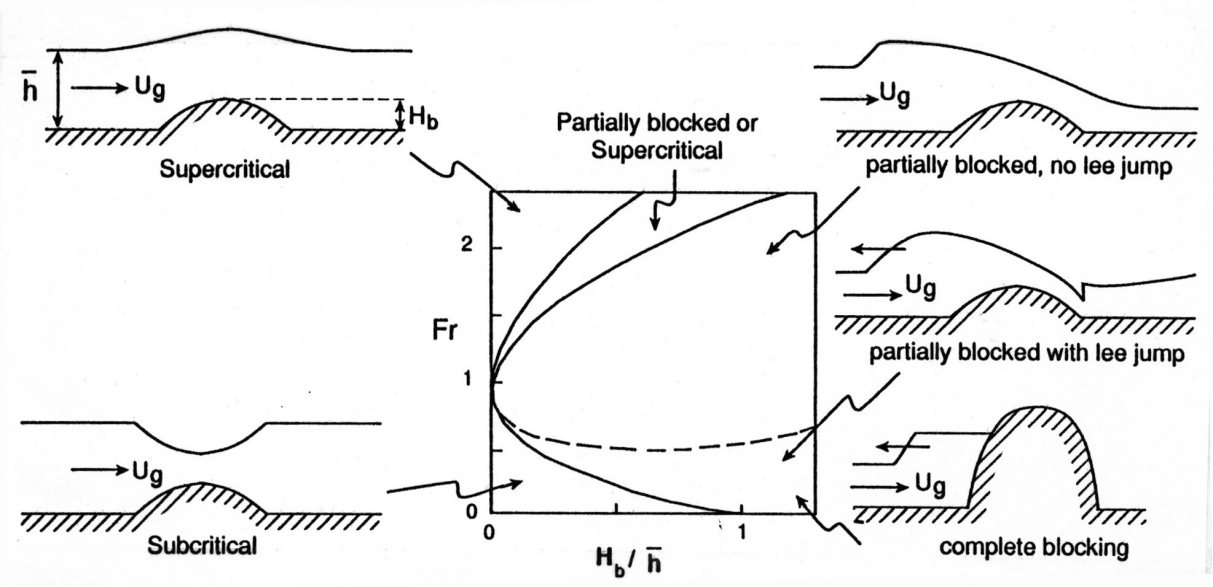

FIGURE 6.3. Regime diagram of the flow of a shallow layer of fluid with constant density over an isolated hill as a function of Froude number far upstream and the non-dimensional height of the hill (adapted from Baines, P.G., 1987: Upstream blocking and airflow over mountains. **Ann.Rev.Fluid Mech.**, 19, 75-97).

According to (6.7), du/dx becomes infinite if $Fr=\pm 1$ and $\left(\frac{dh_s}{dx} - \frac{fv}{g}\left(1 - \frac{u_g}{u}\right)\right)\neq 0$. Assuming for simplicity that $f=0$ and, given the fact that $0<Fr<1$ far upstream, we would expect $du/dx>0$ if $dh_s/dx>0$ and $du/dx<0$ if $dh_s/dx<0$, which is exactly what is observed in **figure 6.2a**. This is an example of so-called **subcritical** flow, for which $Fr<1$.

The other flow regime (for which $Fr>1$) is termed **supercritical**. In this regime we would expect mass convergence and deceleration of the flow on the upstream side of the mountain crest and mass divergence and deceleration of the flow on the downstream side of the mountain crest.

Of special interest are the cases where there is a regime transition, such as when there is a transition from supercritical flow to subcrtical flow in the lee of the mountain giving rise to a so-called **hydraulic jump**. In fact this situation only arrises when the flow is subcritical far upstream and the mountain height is large relative to the fluid depth. This apparently induces acceleration downslope as well as upslope with a subscritical to supercritical transition somewhere near mountain crest and a supercritical to subcritical transition in the lee of the mountain. The second transition gives rise to a hydraulic jump.

The different regimes characterizing single-layer flow over an obstacle in a non-rotating fluid ($f=0$) are summarized in **figure 6.3**. Except for Fr, the relative height of the obstacle also governs the behaviour of the fluid. The diagram presented in **figure 6.3** has been obtained on the basis of theoretical, experimental and numerical investigations carried out by many investigators.

6.3 Severe downslope winds

The hydraulic model has been applied to the atmosphere, in particular to explain the violent downslope winds and turbulence observed in the flow over the Sierra Nevada range in the United States. Intense downslope windstorms are observed frequently in many parts of the world. One of the most well known examples is the so-called "**Bora**" wind occurring along the steep coast of Croatia. This windstorm develops when cold continental air is forced over the coastal mountain range and out over the relatively warm Adriatic Sea. The acceleration of the flow starts already where the mountains begin to rise and continues over the crest and down the other side[172]. The concept of blocking and of transition from subcritical to supercritical flow offers a very plausible explanation of these phenomena. This appears to be confirmed by numerical simulations of two-dimensional continuously stratified flow over a mountain-ridge[173].

Very violent downslope winds have also been observed near Boulder, Colorado. In one case, which is particularly well documented by Lilly (1978)[174], windspeeds of up to 55 m s^{-1} were measured on the eastern slopes of the Rocky Mountains (see **figure 6.4**). The analysis of the potential temperature field for this case, displayed in **figure 6.4b**, suggests that the hydraulic model gives a good first order accurate description of these phenomena.

---

[172] Smith, R.B., 1987: Aerial observations of the Yugoslavian Bora. **J.Atmos.Sci.**, 44, 269-297.

[173] Durran, D.R., 1986: Another look at downslope windstorms. Part I:Development of analogs to supercritical flow in an infinitely deep, continuously stratified fluid. **J.Atmos.Sci**.,43, 2527-2543.

[174] Lilly, D.K., 1978: A severe downslope windstorm and aircraft turbulence event induced by a mountain wave. **J.Atmos.Sci.**, 35, 59-77.

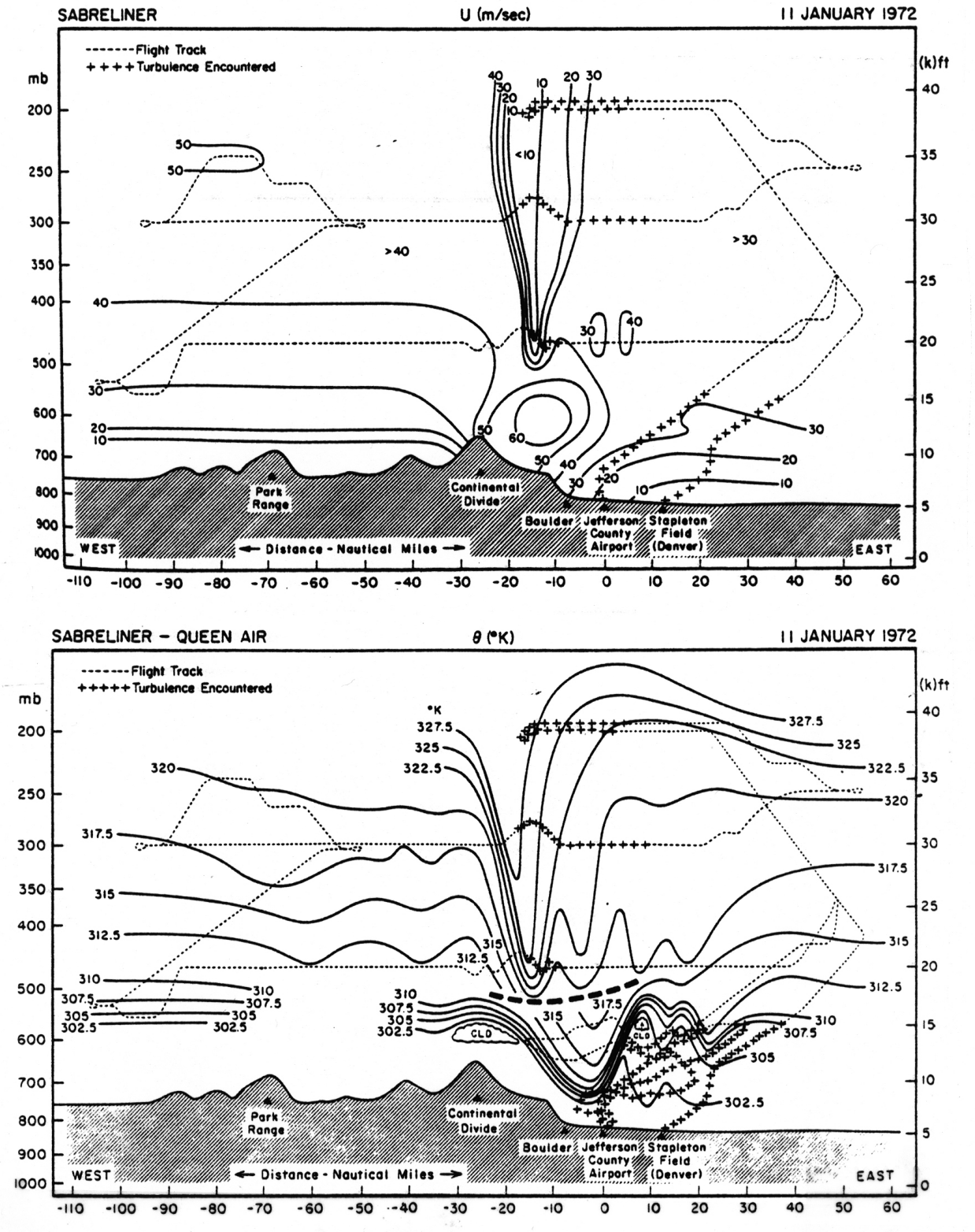

FIGURE 6.4. (a) Analysis of the westerly wind component (m s-1) on 11 January 1972, made from aircraft flight data and radiosondes. (b) Analysis of the corresponding potential temperature field (solid lines). The dashed lines show the aircraft track, with periods of significant turbulence shown by pluses. The heavy dashed line separates data taken by the Queen Air at lower levels before 2200 UT from that taken by the Sabreliner in the middle and upper troposphere after 0000 UT (12 January) (from Lilly, D.K., 1978: A severe downslope windstorm and aircraft turbulence event induced by a mountain wave. **J.Atmos.Sci., 35**, 59-77).

An effect that appears crucial in producing strong downslope winds is the blocking of the low level air-flow by the mountains. If the air cannot flow around the mountain, the pressure upstream from the mountain will rise until the air is able to flow over the crest. Another factor that seems to be of importance is the presence of an inversion layer such as the inversion layer between 500 and 600 mb in **figure 6.4b**. The pressure gradient, which is set up due to the blocking, is confined principally to levels below the inversion. Therefore, only the layer below the inversion is accelerated. **Figure 6.3** demonstrates that the thickness of this layer relative to the mountain height determines the response on the lee-side.

6.4 Gap flows

An analogous situation arises in a valley with a constriction (**figure 6.5a**). Blocking by the constriction can induce a transition from subcritical to supercritical flow leading to continued acceleration of the air down the valley when the valley-width increases. It has been hypothesized[175] that this effect produces the famous "**Mistral**" wind in the Rhone valley in southern France. The Mistral is mostly observed in circumstances with a northerly "geostrophic" airflow, which is blocked by the Alps (**figure 6.6**). Observations show that winds are relatively weak upstream from the constriction, near Valence, while there is a sudden increase in the wind downstream from the constriction. The acceleration continues until a maximum wind speed is reached about 100 km downstream from Valence (**figure 6.5b**). A sudden transition back to calmer conditions, similar to a hydraulic jump, is frequently observed near Nimes, about 150 km from Valence. Observations seem to indicate that a potential temperature inversion at relatively low levels is required to produce violent mistral winds.

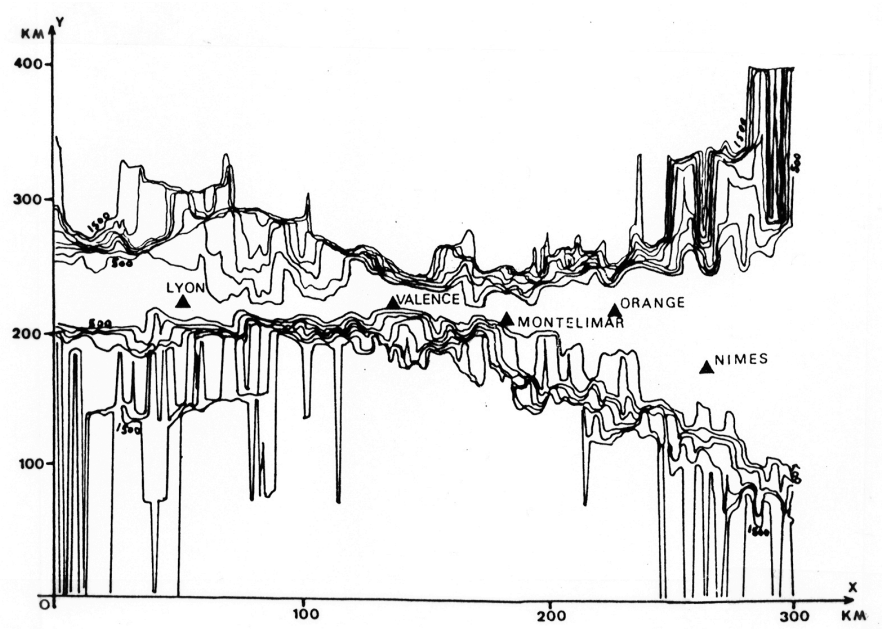

FIGURE 6.5a. Height of the Rhone valley walls. Isopleths are seperated by 100 m using the orography given on a grid with a 1 km mesh (from Pettre, P., 1982: On the problem of violent valley winds **J.Atmos.Sci.**, 39, 542-554).

[175]Pettre, P., 1982: On the problem of violent valley winds **J.Atmos.Sci.**, 39, 542-554.

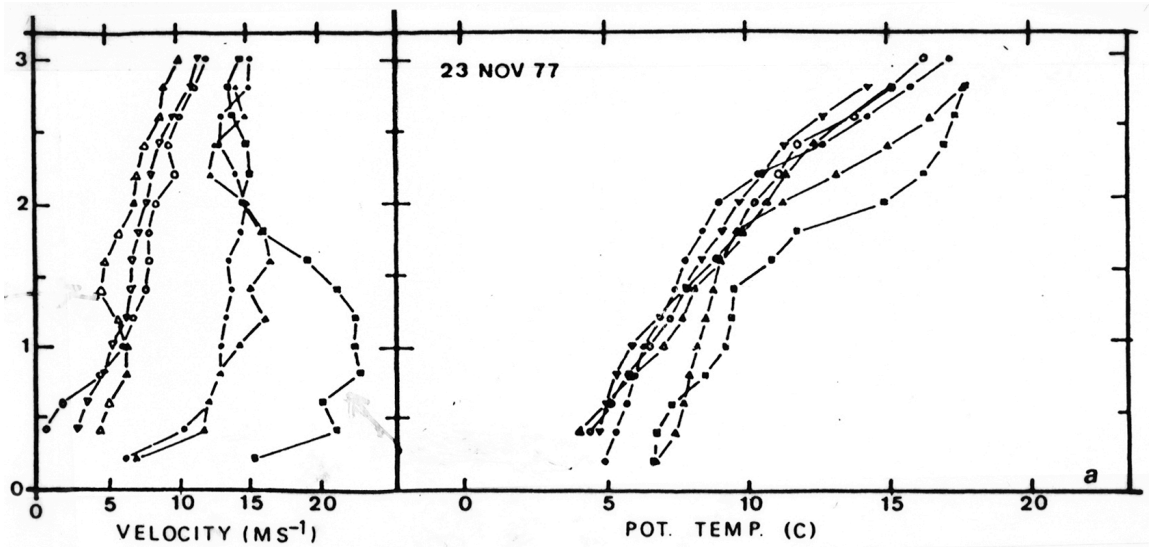

FIGURE 6.5b. 10-minute average wind speed and potential temperature profiles at Feurs (○), Cuisery (△), Satolas (Lyon) (▽), Valence (●), Orange (■) and Nimes (▲) for 23 November 1977 (from Pettre, P., 1982: On the problem of violent valley winds **J.Atmos.Sci.**, 39, 542-554).

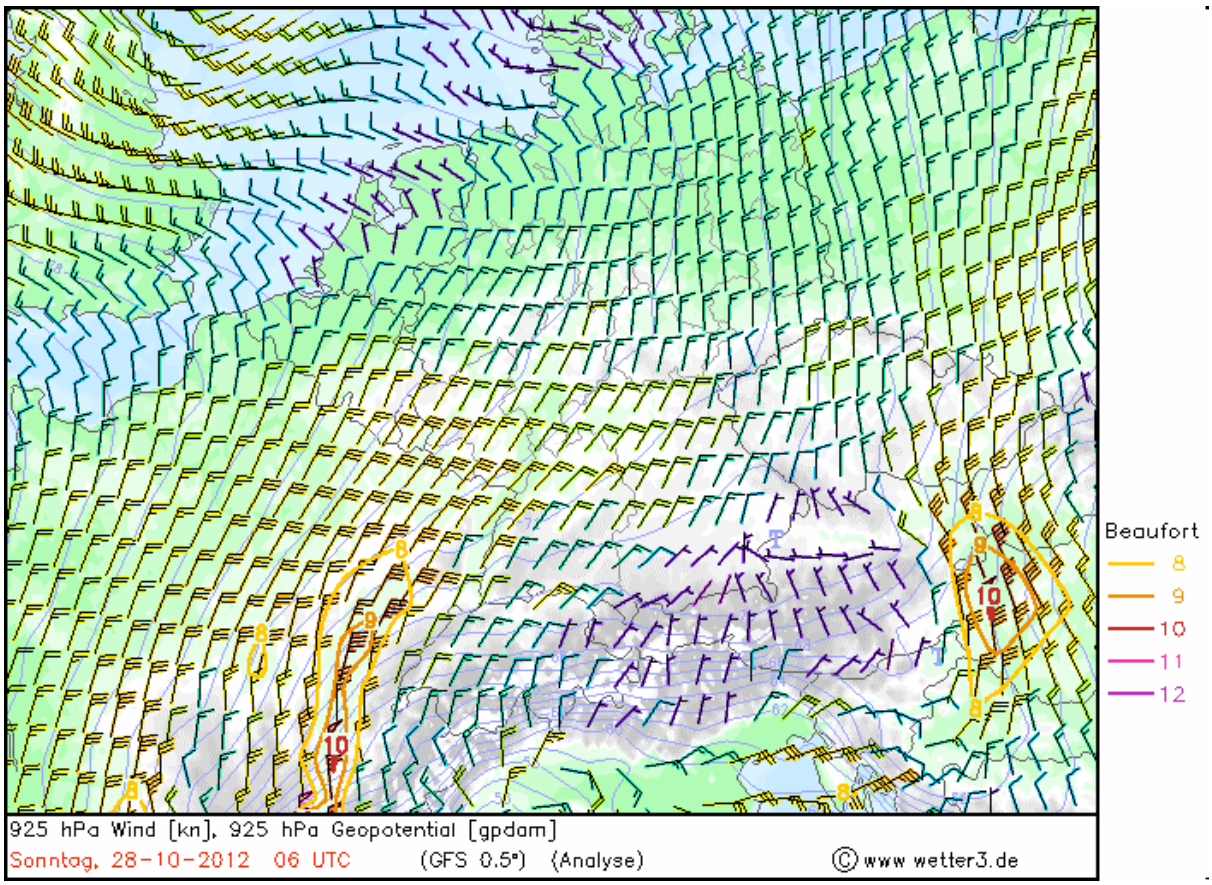

FIGURE 6.6. Winds at 925 hPa (about 700 m a.s.l.) with wind speeds greater than 8 Beaufort indicated by contouring, in a case of blocking of the air-flow from the north by the Alps. The air is funneled through the large valleys to the west and east of the Alps. The Bora is observed to the south-east of the Alps along the Adriatic Sea coast. The mistral is observed in the Rhone Valley and the Gulf of Lion.

6.5 Katabatic winds

One very conspicuous aspect or property of downslope winds is that some are warm and others are cold. The Bora and Mistral are relatively cold winds while the well-known **Foehn**, occuring in the lee of the Alps, is warm (**figure 6.7**). The warmth of the Foehn has been attributed in the past to release of latent heat in the air rising from the ground at the upwind side of the mountain range. Doubt has been cast on this hypothesis[176]. The mechanism producing warm Foehn is probably identical to the mechanism producing the cold Bora. Although the Bora is felt as a cold wind, this is only relative to the originally warm air found along the Adriatic coast. The Foehn is felt as a warm wind because it replaces a relatively cold layer of air near the ground in the lee of the Alps. In all cases the air reaching the ground in the lee of the mountain range is potentially warm air coming from higher altitudes (**figure 6.4b**).

Mistral and Bora are sometimes referred to as a **katabatic wind**. The term "katabatic" is of Greek origin from *katabatikos*, meaning to go down. In most general sense, any wind blowing down an inclined surface can be classified as a katabatic wind.

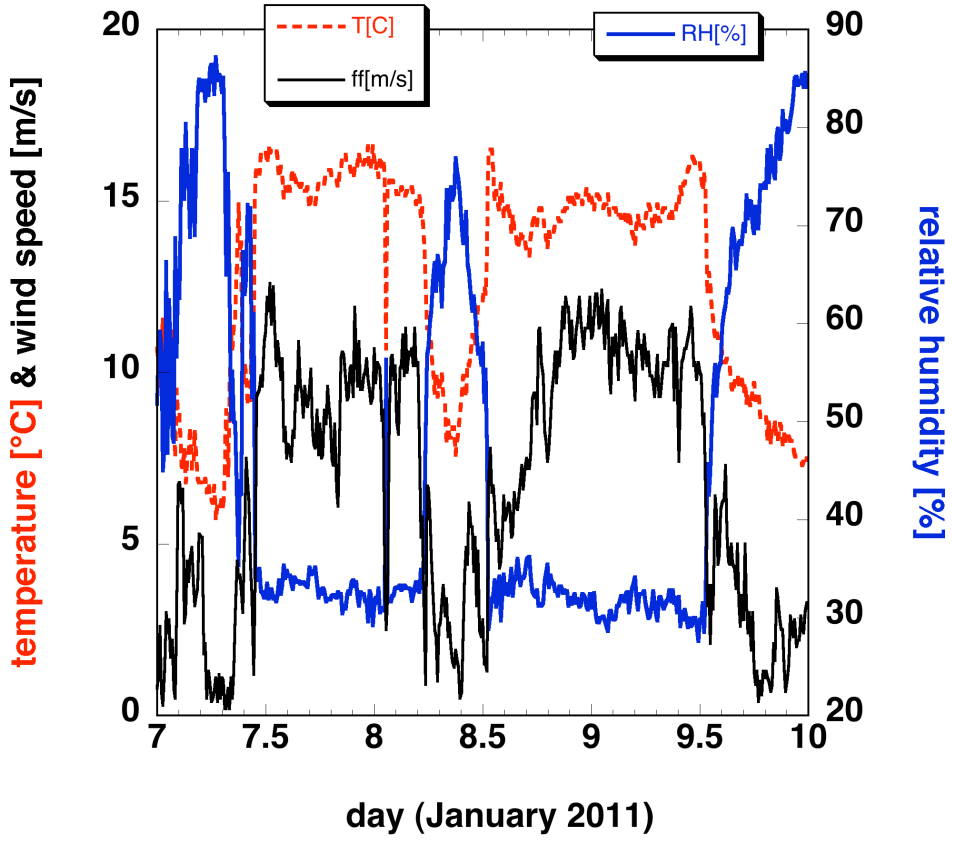

FIGURE 6.7. Ten minute mean wind speed (ff), temperature and and relative humidity (RH) at Altdorf on three days in January 2011. Altdorf is located in a valley on the north side of the Alps to the south of Zurich. The valley (Reusstal) is oriented in south-north direction, perpendicular to the row of main peaks of the Alps, and is separated by only one single ridge of high mountain peaks from the south side of the Alps. When the Foehn is blowing the relative humidity is very low (about 30%) and the temperature is relatively high. Data is from MeteoSwiss (thanks to Michael Sprenger and Hilke Lentink).

[176]Siebert, P., 1990: South Foehn studies since the ALPEX experiment. **Meteorol.Atmos.Phys.**, 43, 91-103.

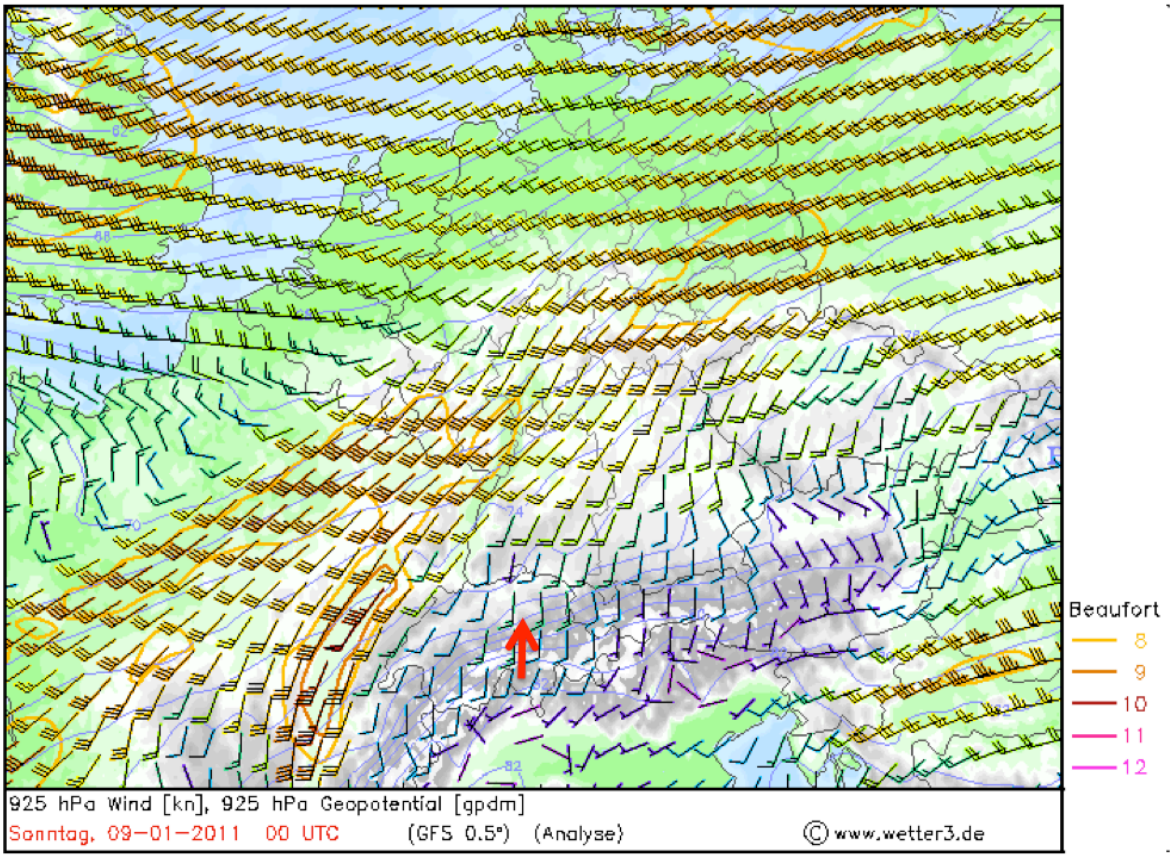

FIGURE 6.8. Geopotential height (labeled in dm) and winds at 925 hPa on 9 January 2011 (see also **figure 6.7**), again showing the funneling of air from the south through the Rhone valley, west of the Alps (see also **figure 6.6**). Also noteworthy is the gradient from south to north of about -60 m in the geopotential height across the Alps. The location of Atdorf is indicated by the red arrow.

Katabatic winds are best developed over the great ice sheets of Antactica and Greenland. The persistent radiative cooling over Antarctica, especially during the dark polar night, causes the surface to become colder than the free atmosphere by as much as 30–35 K. The surface layer air becomes negatively buoyant with respect to the free atmosphere. The cold air that flows down the slope of the ice sheet represents the notorious Antarctic katabatic winds. The size of the continent and the persistent surface cooling in winter enables the Coriolis effect to deflect the katabatic winds in the cross-slope direction. Channeling of air due to valley-shaped topography can locally enhance katabatic wind speeds. This is particularly true for Adélie Coast (**figure 6.9**) where the strongest winds on Earth are observed, annual mean wind speeds frequently exceed 15 m s^{-1}.

Figure 6.10 shows the modeled July surface layer wind vector and directional constancy averaged over the period 1980–93. The directional constancy, dc, is defined as the ratio of the time-mean to vector-mean wind speed:

$$\mathrm{dc} \equiv \left(\bar{u}^2 + \bar{v}^2\right)^{1/2} \left[\overline{\left(u^2 + v^2\right)^{1/2}}\right]^{-1}$$

The bar denotes a time mean. The modeled surface layer wind velocities (9–14 m s^{-1}) and dc (0.9–0.95) are highest in the zone where the slope of the ice sheet is steepest, while weak winds and low dc are found over the domes of the interior ice sheet.

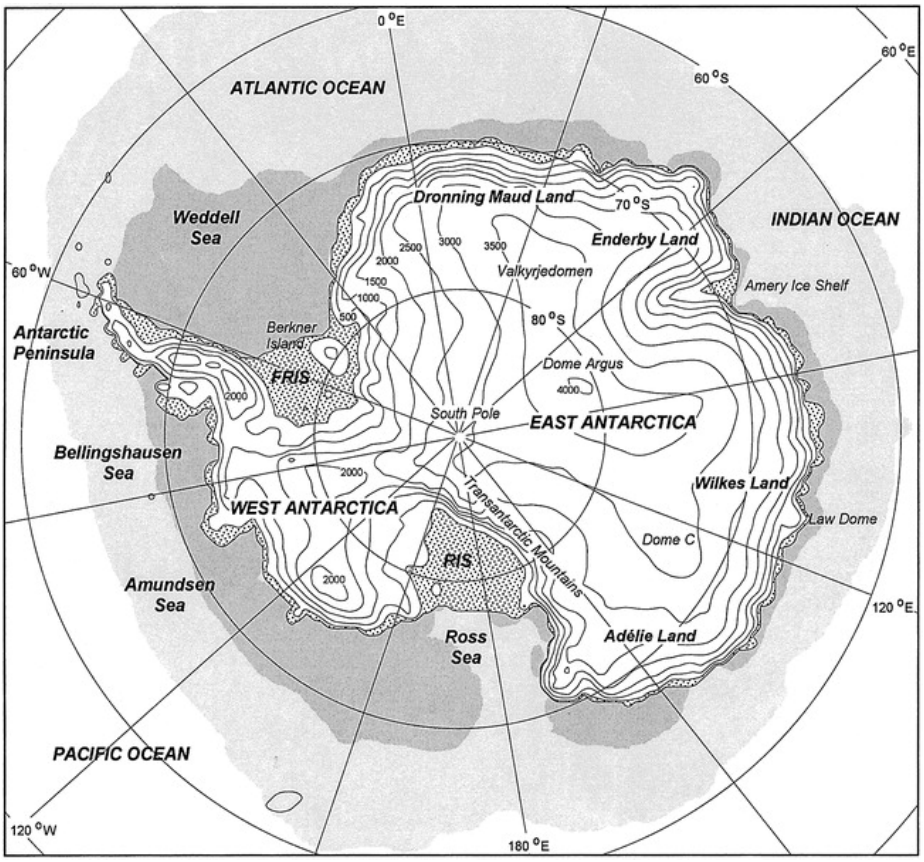

FIGURE 6.9. Topographical features of Antarctica. Ice shelves (stippled); average July sea ice extent (light shaded); average January sea ice extent (dark shaded). Surface elevation (m above mean sea level) is contoured every 500 m. RIS: Ross Ice Shelf; FRIS: Filchner–Ronne Ice Shelf. From van den Broeke, M.R., and N.P.M. van Lipzig, 2003: Factors controlling the near-surface wind field in Antarctica. **Mon.Wea.Rev., 131**, 733-743.

6.6 Stability of stratified shear flow and nonhydrostatic resonant lee-waves

Early studies of disturbances produced by mountains were directed towards finding a theory which could explain the relatively small-scale non-hydrostatic **lee-waves frequently visible as a series of parallel cloud bands** (with a spacing in the order of 10 km) near mountain ranges (**figure 6.1**). Because the amplitude of these phenomena is relatively small, linear (Boussinesq-) theory, as described in section 2.2, is adopted to investigate this problem. Since the horizontal structure of the wave field is determined by the structure of the mountain, which is not necessarily sinusoidal, this structure is not specified a priori. In the following the theory is presented as a problem.

PROBLEM 6.1. Buoyancy waves in a stationary flow over two-dimensional topography[177].

This problem consists of many steps, which will lead us to the dependence of the structure of mountain generated buoyancy waves on the mean flow and the mean temperature

177 based on theory described by Durran (1986) (Mountain waves. In **Mesoscale Meteorology and Forecasting**. American Meteorological Society, Boston. 793 pp. (p. 472-492)).

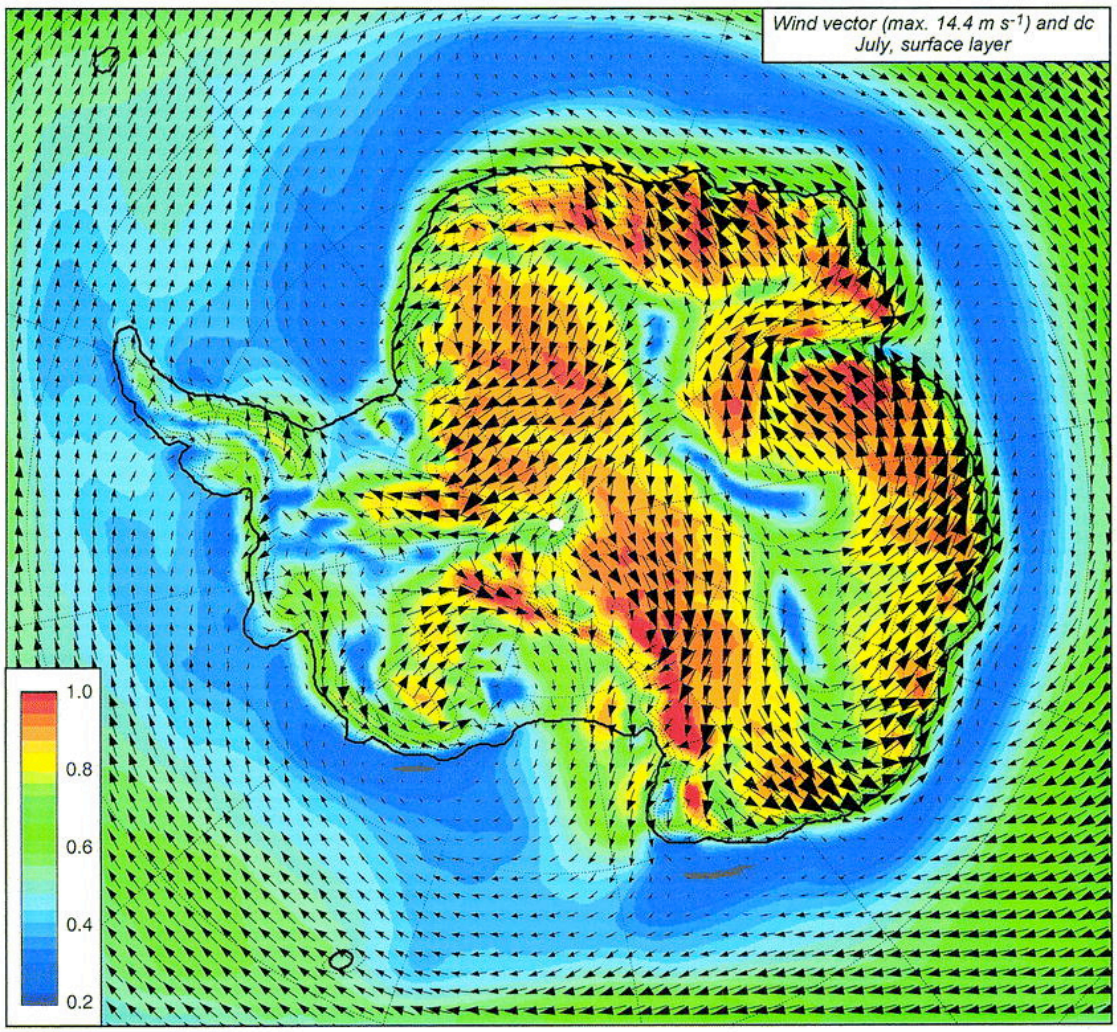

FIGURE 6.10. Average July (1980–93) modelled surface layer wind vector (arrows) and directional constancy (colors). From van den Broeke, M.R., and N.P.M. van Lipzig, 2003: Factors controlling the near-surface wind field in Antarctica. **Mon.Wea.Rev., 131**, 733-743.

stratification. The two-dimensional topography consists of a series of ridges parallel to the y-axis. The mean state is given by a flow $u_0(z)$ in the x-direction and a potential temperature distribution $\theta_0(z)$. We will make the Buossinesq approximation for "shallow" flow (see chapter 3) and neglect the Coriolis force. We can linearise the equations about the mean state if the orography is "gentle". This results in a system of equations, including the effect of the mean flow, $u_0(z)$, similar to eqs (3.16-3.20). Although we assume a variation in velocity with height and so imply a thermal wind, no horizontal variation of potential temperture is assumed. The wavelengths considered are such that the Earth's rotation can be ignored in its effect on the disturbance. For normal wind speeds (order 10-30 m/s) this restricts discussion to wavelengths less than 10-100 km.

(a) The flow-pattern is stationary with respect to the topography. This steady state assumption implies that $\partial(...)/\partial t=0$. This gives a system of 4 equations with 4 unknowns (u, w, P and B) with $P=\theta_m \Pi$ and $B=\theta g/\theta_m$. Reduce this system of equations to one equation for w.

(b) Define the terrain profile as an infinite set of ridges as follows:

$$h(x) = \mathrm{Re}\left\{h_0 \exp(ikx)\right\},$$

where h_0 is the complex amplitude. Because w=dh/dt, at the Earth's surface an expression for $w(x, 0)$ can be derived. Show that an approximation to this expression is

$w(x,0) \approx \mathrm{i}u_0 h_0 k \exp\{\mathrm{i}kx\}$.

(c) The equation for $w(x,z)$ derived in (a) has a solution of the form $w(x,z)=W(z)\exp(\mathrm{i}kx)$. Substituting this solution yields an equation of the form

$$\frac{d^2W}{dz^2} + \left(l^2 - k^2\right)W = 0, \tag{6.9}$$

where l is the **Scorer parameter**[178]

$$l^2 \equiv \frac{-\mathrm{D}^2 u_0}{u_0 - c_x} + \frac{k^2 N^2}{\alpha^2 \left(u_0 - c_x\right)^2}, \tag{6.10}$$

where $\mathrm{D}^2 = d^2/dz^2$. What is the solution to this equation?

(d) What is the character of the solution if $\mu^2 \equiv \left(l^2 - k^2\right) > 0$ and if $\mu^2 \equiv \left(l^2 - k^2\right) < 0$?

(e) Write down the solution in these two cases and draw the streamlines for each case. Assume h_0 is real. Do the phase lines of the wave tilt upstream or downstream with height in the case of broad ridges ($k^2 < l^2$)?

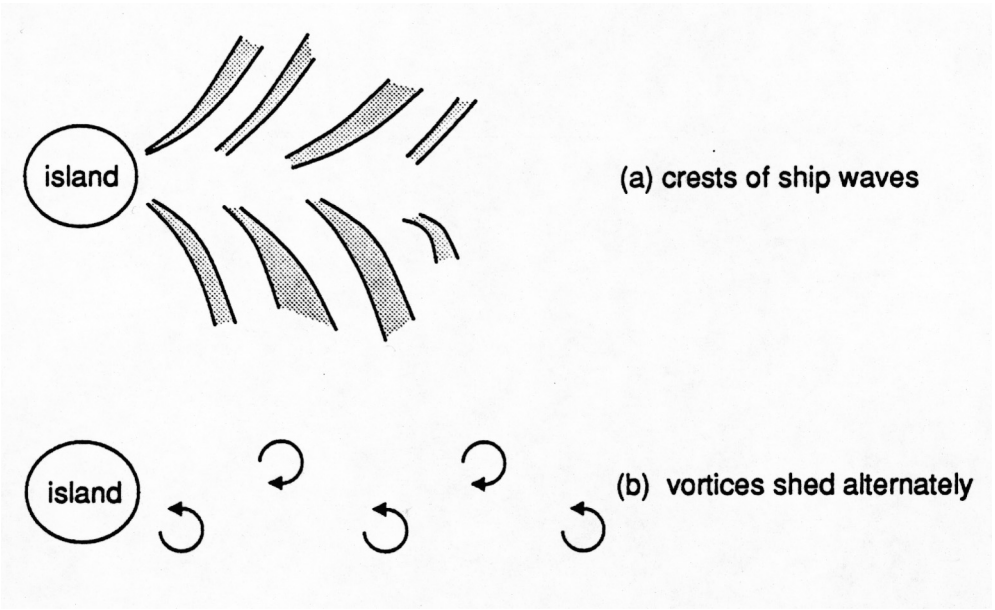

FIGURE 6.11 (a) The crests of "ship" waves behind an isolated obstacle at high Froude numbers. (b) Vortices shed alternately by the same obstacle at low Froude numbers.

[178] Scorer, R.S., 1949: Theory of waves in the lee of mountains. **Q.J.R.Meteorol.Soc.**, 75, 41-56.

6.7 Flow around mountains

When air encounters a three-dimensional obstacle, it can flow both over and around the obstacle. If the fluid is stably stratified, a so-called "**dividing streamline**" can be formed which separates the upper layer flowing over the hill from the lower layer flowing around the hill. For a simple background flow with constant u_0 and constant N, the dividing streamline height, h_c, is given by

$$h_c = H_b\left(1-"Fr"\right) , \tag{6.11}$$

where "Fr" is defined in yet another way according to

$$"Fr" \equiv \frac{u_0}{NH_b} , \tag{6.12}$$

where H_b is the maximum height of the obstacle[179]. Here the Froude number "Fr" has been placed between inverted commas in order to distinguish it from the other Froude numbers defined in (6.1) and (6.8). There have been some critical comments in the literature on the many definitions of the Froude number used in different contexts[180]. It might be best to reserve the term, Froude number, for the ratio of the flow velocity to the phase speed of some wave, as in (6.8). The "Froude number" defined in (6.12) clearly does not meet this requirement. Rather, it is a measure of the ratio of the mean velocity to the perturbation velocity induced by the mountain, and thus a measure of nonlinearity. We will not decide here which is best definition of Fr, since the different definitions are still used by the different specialists studying flow over and around mountains. Perhaps it is best to refer to the inverse of "Fr" as the non-dimensional mountain height or normalized moutanin height.

According to eq. 6.11 a dividing streamline will only exist for "Fr"<1. The air below the height, h_c, will have insufficient kinetic energy to overcome the potential energy barrier, induced by the stable stratification, and to flow over the mountain top. The air flowing around the obstacle will form counter-rotating vortices in the lee, while the air flowing over the obstacle will produce gravity waves. These two characteristic flow patterns are easily recognized in the cloud pattern on satellite photographs[181]. In high "Froude number" flow over relatively steep islands the gravity waves are frequently seen as so-called "**ship waves**" (see **figure 6.11a**). In low "Froude number" flow, **lee-vortices** form especially when there is a strong potential temperature inversion below the mountain-top. These vortices are shed alternately, forming **vortex streets** (see **figure 6.11b**). The similarity with the Karman vortex streets, observed in fluid flow behind a cylinder in the laboratory is remarkable[182]. It is, however, not entirely clear whether the two phenomena can be attributed to the same mechanism. For the Karman vortices the production of vertical vorticity is due to the viscous stress at the side walls of the cylinder and the subsequent viscous boundary-layer separation.

---

[179] Etling, D., 1989: On atmospheric vortex streets in the wake of large islands. **Meteorol.Atmos.Phys.**, 41, 157-164.

[180] Baines, P.G., 1987: Upstream blocking and airflow over mountains. **Ann.Rev.Fluid Mech.**, 19, 75-97.

[181] Scorer, R.S., 1986: **Cloud Investigation by Satellite**. Ellis Horwood Series in Environmental Science.

[182] Kundu, P.K., 1990: **Fluid Mechanics**. Academic Press inc., 638 pp.

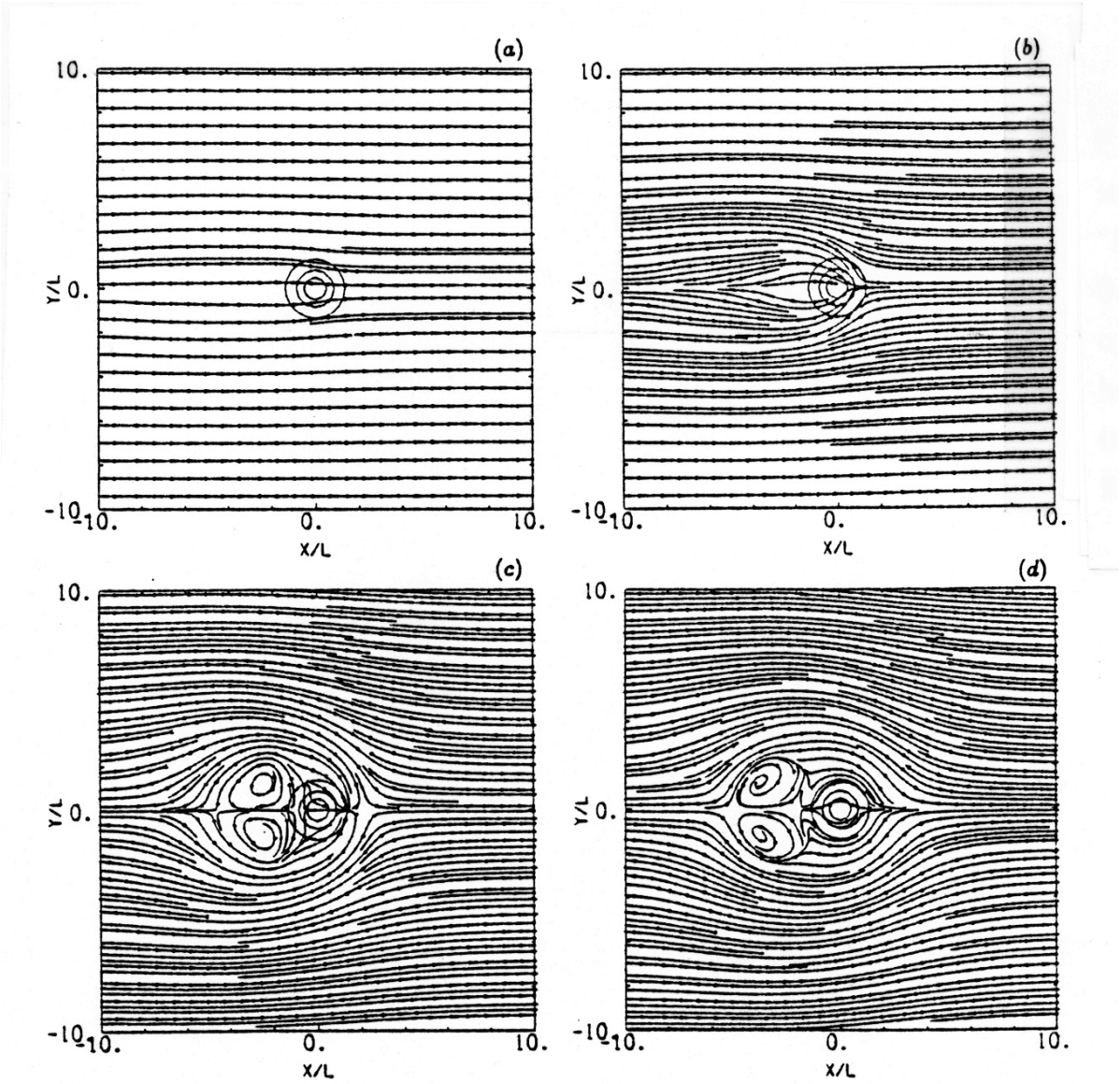

FIGURE 6.12. Steady state streamlines at the lower surface for "Fr" = (a) 2.2, (b) 0.66, (c) 0.22, (d) 0.055. Concentric contours in the centre of the domain represent the height of the obstacle with contour interval $0.25H_b$ (Smolarkiewicz and Rotunno, 1989). H_b= 0.12 L .

Laboratory experiments have revealed vortex shedding in a stably stratified flow around obstacles with slopes of 1/4 to 2. Because the steepest islands have slopes of 1/5 or less, the experimental results cannot be carried over directly to the atmosphere[183].

By numerical simulation stress-free stratified flow past a bell-shaped (round) three-dimensional hill, neglecting the effect of the earth's rotation) it can be shown that lee-vortices are produced only when "*Fr*"<0.5 (**figure 6.12**). In **figure 6.13** it can be seen that gravity waves are produced only when "*Fr*" is large. The domain is probably too small to verify whether the wave crests form a ship wave pattern or to investigate vortex shedding[184].

---

[183] Etling, D., 1990: Mesoscale vortex shedding from large islands: A comparison with laboratory experiments of rotating stratified flows. **Meteorol.Atmos.Phys.**, 43, 145-151.

[184] Smolarkiewicz, P.K., and R. Rotunno, 1989a: Low Froude number flow past three-dimensional obstacles. Part I: baroclinically generated lee vortices. **J.Atmos.Sci.**, 46, 1154-1164.

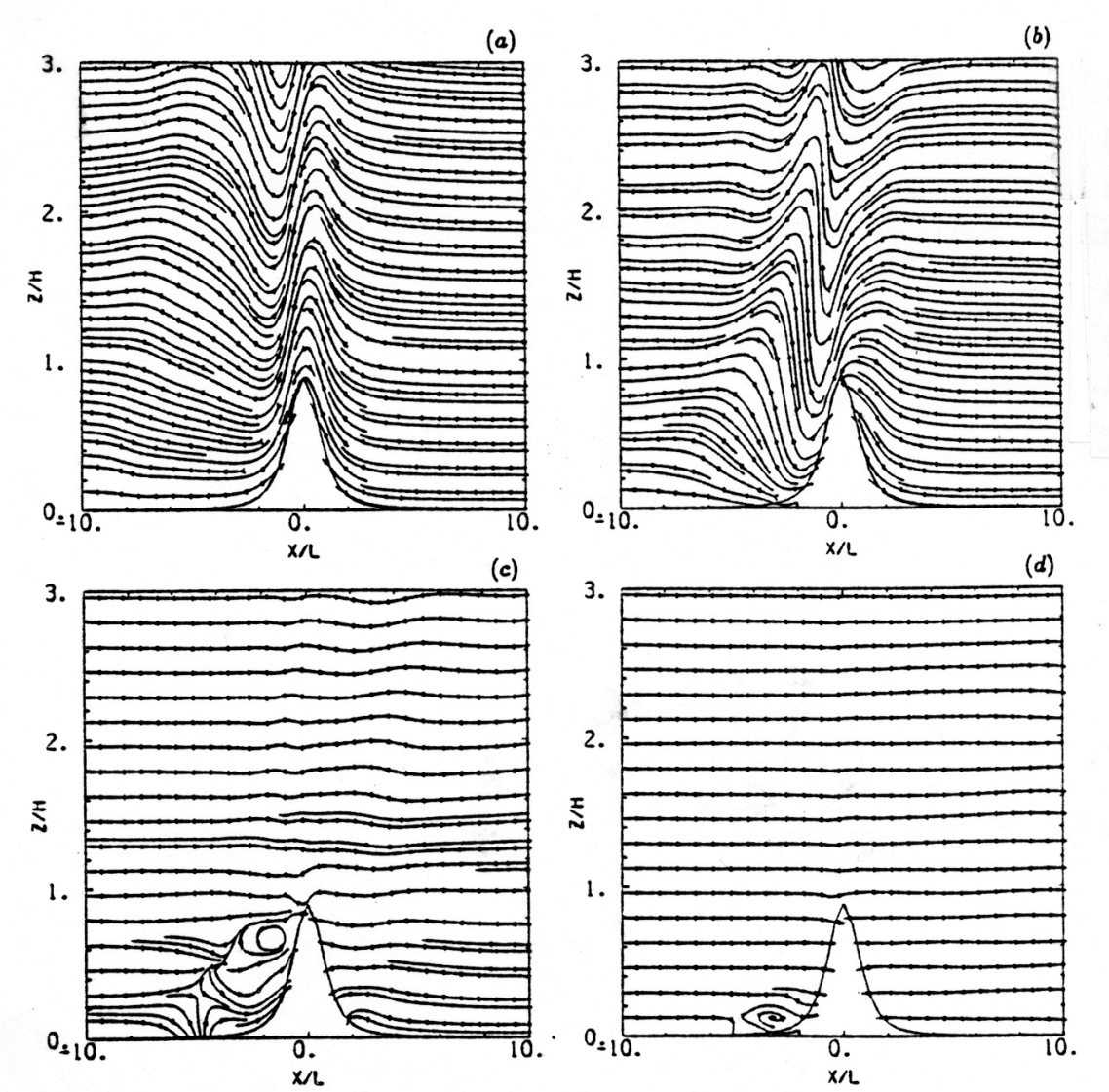

FIGURE 6.13. Steady state streamlines in a vertical cross section through the centre plane for "Fr" = (a) 2.2, (b) 0.66, (c) 0.22, (d) 0.055 (Smolarkiewicz and Rotunno, 1989). H_b= 0.12 L .

Later studies have shown that the shedding of vortices is due to a hydrodynamic instability, which results from the presence of potential vorticity in the wake of the obstacle. This potential vorticity is created due to internal dissipation and diffusion in the fluid. Dissipation occurs in a compact region of breaking gravity waves slightly downstream of the mountain crest[185].

A characteristic feature of low "Froude number" flow is the zone of **flow-reversal** on the windward side of a three-dimensional obstacle. Here too, numerical model experiments indicate quite clearly that frictional boundary layer separation is not needed for upwind stagnation and flow-reversal. The flow-reversal is only observed when the aspect ratio, β (across-stream length divided by the along-stream length), is greater than one. Lee-vortex

---

Smolarkiewicz, P.K., and R. Rotunno, 1990: Low Froude number flow past three-dimensional obstacles. Part II: upwind flow reversal zone. **J.Atmos.Sci.**, 47, 1498-1511.

[185]Schär, C., and D.R. Durran, 1997: Vortex formation and vortex shedding in continuously stratified flows past isolated topography. **J.Atmos.Sci.,** 54, 534-554.

formation seems to be independent of β, although the lee-vortices become much larger and more marked when β increases.

Topography can influence the flow on the meso-scale in many ways, especially in combination with diabatic heating (thermally induced valley and slope winds; katabatic winds) and friction.

6.8 Lee-cyclogenesis

The regions exhibiting the most intense **cyclogenesis** (=the formation of a cyclone) typically lie adjacent to mountain regions, such as to the east of the Rocky-mountains and to the south of the European Alps (**figure 6.14**). Cyclogenesis to the south of the Alps has been investigated extensively. It typically occurs when cold air approaches the Alps from the north-west. Below the 700 hPa level this cold air is blocked by the mountains and is forced to flow around, especially through the Rhone valley to the west. Above 700 hPa the cold air continues its journey southward over the Alps. This effect generates extreme potential instability over the Po valley in Italy in the summer season, when the valley is filled (at low levels) with very humid and warm air. The blocking of the cold air also leads to positive surface pressure tendencies to the north of the Alps and negative surface pressure tendencies to the south. In particular, an isallobaric minimum is generated over the Gulf of Genoa (**figure 6.15a**). The attendant isallobaric wind (**figure 6.15b**)[186] is convergent in this region and, thus, leads to cyclogenesis at levels below the mountain crest. In the example shown in **figure 6.15a** cyclone of appreciable intensity forms within 12 hours at 850 hPa (**figure 6.15c**). The flow associated with the newly formed cyclone distorts or deforms the front as happens in a growing baroclinic wave (chapter 10), i.e. there is warm air advection on the eastern side and cold air advection on the western side. We will see in chapter 9 that this pattern of temperature advection is advantageous for further growth of the cyclone. In fact, the Alpine mountain range itself distorts the front and this in itself may induce cyclogenesis. It is probably no coincidence that cyclogenesis is usually observed in regions where the thermal or physical properties of the earth's surface promote the horizontal distortion of isentropes, such as near coasts and near mountains and hills (**figure 6.14**). Therefore, it seems that lee cyclogenesis is initiated due to isollabaric effects induced by blocking of cold air and is subsequently intensified by static destabilization (due to cold air passing the ridge at upper levels) and by baroclinic effects (rotation of the isentropes). Probably latent heat release in clouds over the relatively warm Mediterranean Sea also contributes to the intensification of the lee-cyclone. The most intense cyclogenesis to the south of the Alps is observed in northerly flow when a so-called "**positive potential vorticity anomaly**" approaches the Alps from the north. The significance of latent heat release and potential vorticity in the process of cylogenesis will become clear in chapter 7 (Box 7.2).

6.9 Stationary orographic Rossby waves

The standard textbook model for large-scale zonal (west-east) flow over orography is based on the principle of conservation of potential vorticity following the adiabatic motion of fluid columns over an infinite ridge (figure 6.13). If we adopt the one-layer model, described in section 6.2, and assume that there is a uniform zonal flow with relative vorticity, ζ=0

[186] See section 1.34 for the definition of isallobaric wind.

upstream of the mountain barrier, we can use this conservation principle to deduce some qualitative features of the response of the zonal flow to the orography. Potential vorticity within the context of this model is defined as

$$\zeta_{pot} = \frac{\zeta + f}{h}.$$

If we neglect the effect of upstream blocking we can immediately say that as the fluid column begins to mount the barrier its depth decreases. The relative vorticity, ζ, must than become negative. The air column thus acquires anticyclonic curvature and moves southward as shown in figure 6.13. When the air column has passed over the mountain and returned to its original depth, it will be south of its original latitude so that the Coriolis parameter, f, (we now assume that f depends on latitude) will be smaller and the relative vorticity must be positive. Thus, the streamlines will curve poleward. The column will then move downstream conserving potential vorticity by following **a wavy constant vorticity trajectory in the horizontal plane**. This wave phenomenon is referred as a **Rossby wave** and, since the wave is excited by orography, it is called an **orographic Rossby wave** in this case.

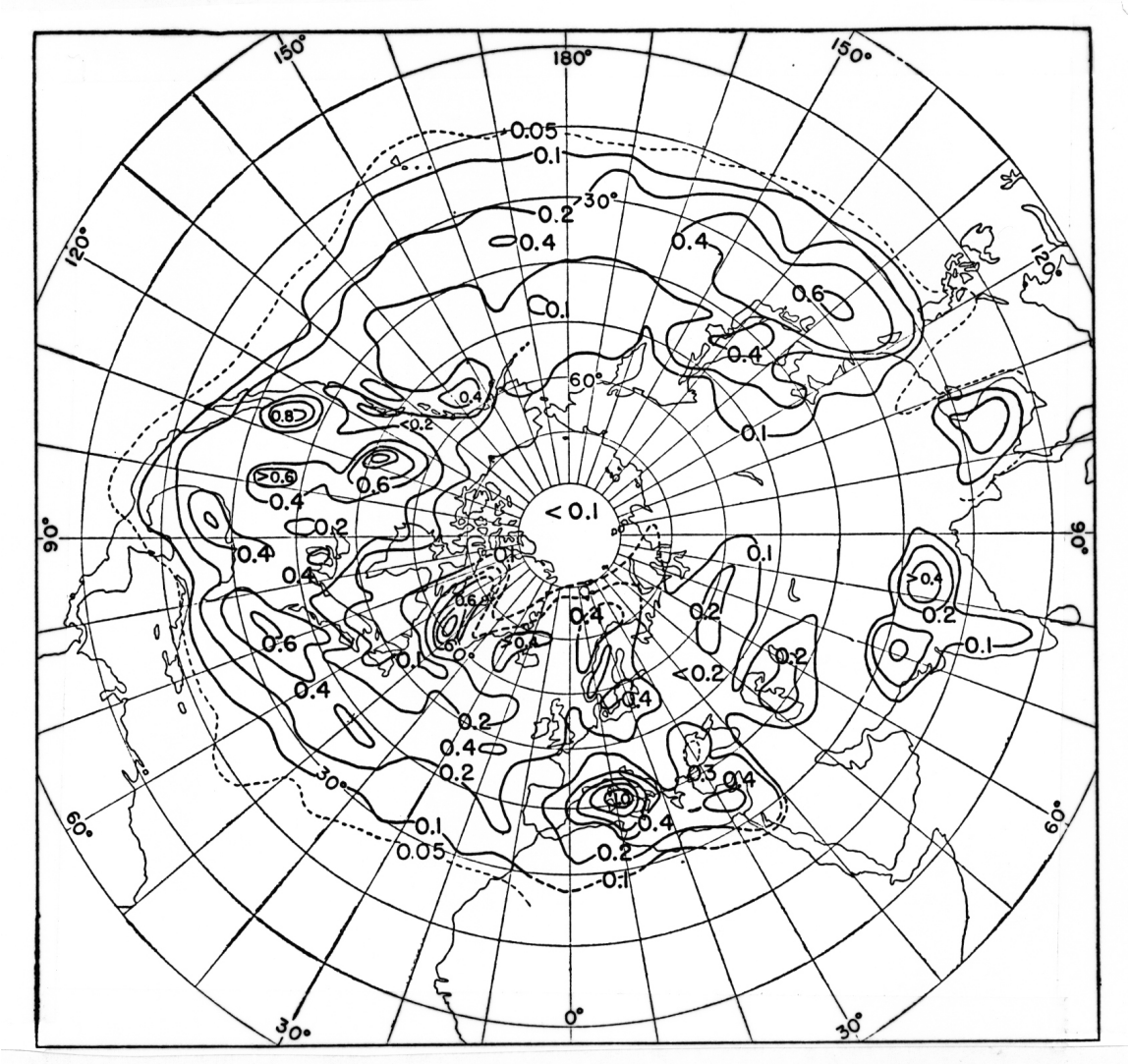

FIGURE 6.11. Percentage frequency of occurrence of cyclogenesis in squares of 100000 km2 in winter (1899 to 1939) (from Petterssen, S., 1956: **Weather Analysis and Forecasting**. Second edition. MacGraw-Hill).

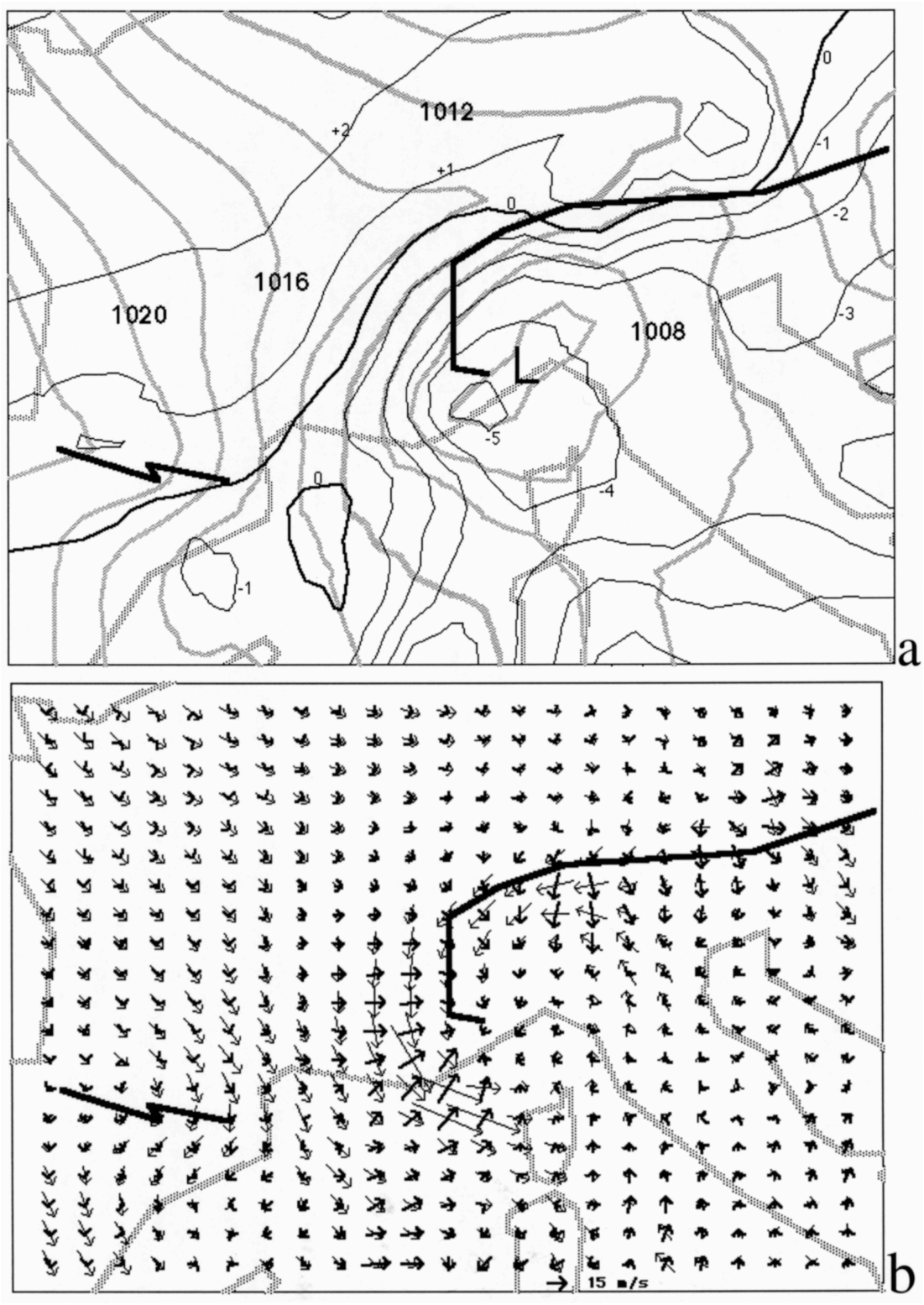

FIGURE 6.12. **(a) Sea level isobars** (thick grey lines, labeled in hPa) and sea level isallobars (thin solid lines, labeled in hPa per 3 hours), November 6, 1999, 12 UTC. **(b) isallobaric wind (bold arrows)** at sea level between 6 and 12 UTC on November 6, 1999 and **geostrophic wind (thin arrows)** at 12 UTC, November 6, 1999. Analysis is based on an interpolation of the surface observations to a "lat-lon"-grid of 20 by 23 points with an interval 0.75° in the zonal direction and 0.5° in the meridional direction. The boundaries of the domain shown are at 2°W, 16°E, 50°N and 39.5°N. The letter "L" marks the centre of the incipient lee cyclone at sea-level. The thick black line marks the mountain ridge higher than 2000 m.

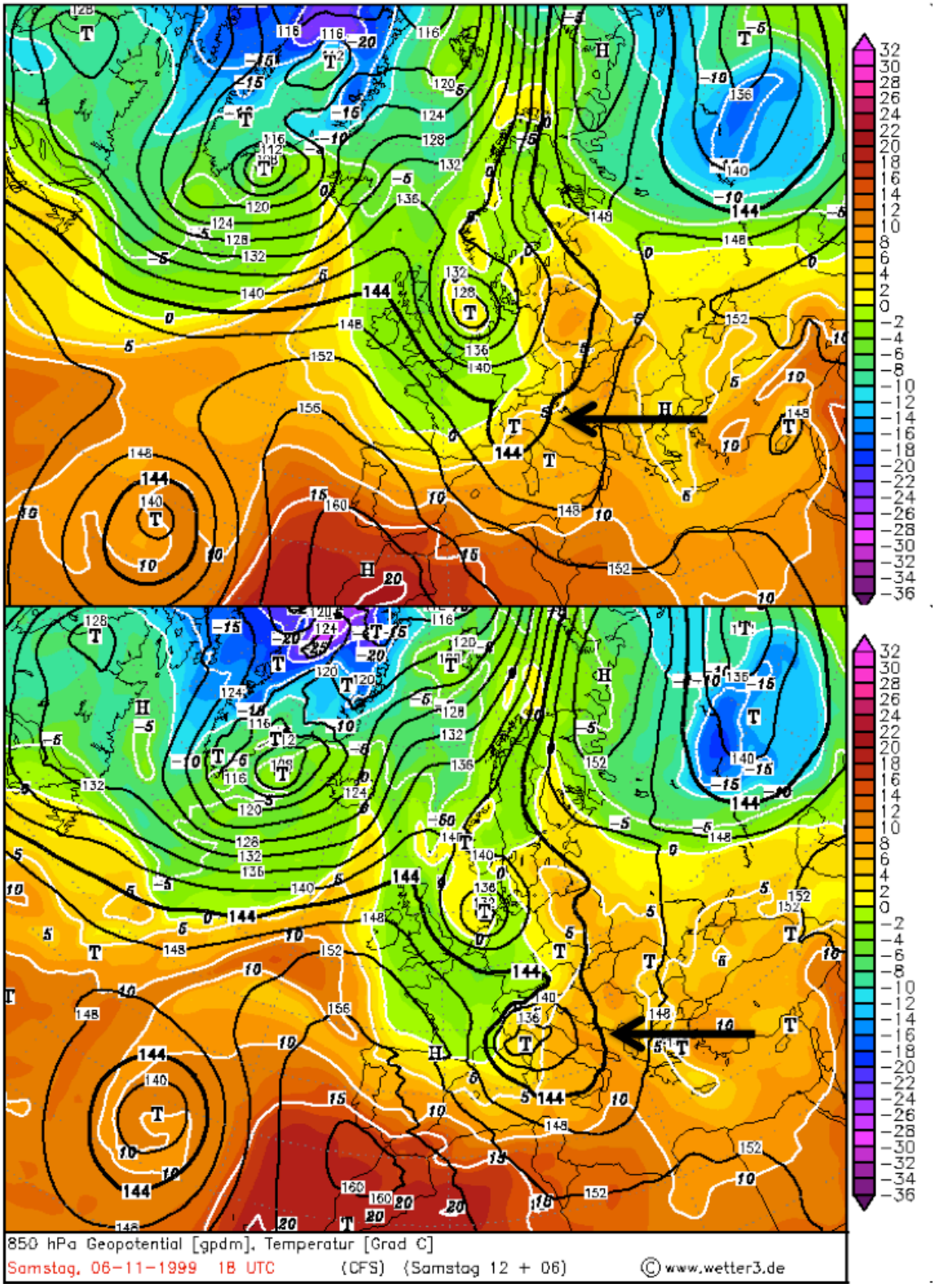

FIGURE 6.12c. Distribution of temperature (in colour) and height (black contours) at 850 hPa during an episode of lee-cyclogenesis over the Gulf of Genoa on 6 November 1999. Upper panel is the analysis of 12 UTC; lower panel is the analysis of 18 UTC. Height is labeled in dm and temperature is labeled in °C. The significance of warm and cold advection for cyclogenesis is explained in chapters 9 and 10. Source of picture: http://www.wetter3.de/Archiv/.

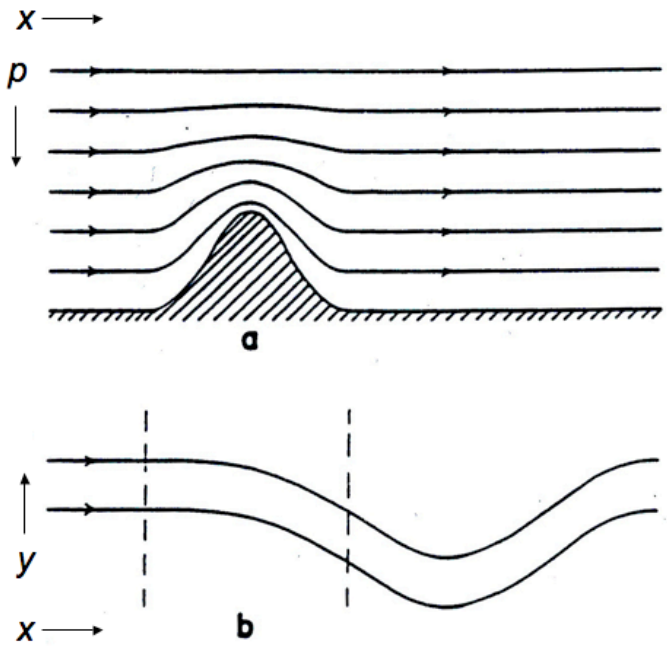

FIGURE 6.13. (a) Height-longitude cross-section and (b) plan view of streamlines for stationary disturbance created by flow of an initial zonal current across a large scale mountain barrier in the northern hemisphere (from Holton, J.R., 1993: The second Haurwitz Memorial Lecture: Stationary Planetary Waves. **Bull.Amer.Meteorol.Soc.**, 74, 1735-1742).

In order to make the above arguments more quantitative, we make the **rigid lid approximation** (**figure 6.14**) by assuming that

$$h = H(y) - h_s(x) \tag{6.13}$$

This implies that blocking effects are ruled out. The continuity equation (6.3c) then becomes

$$\frac{\partial hu}{\partial x} + \frac{\partial hv}{\partial y} = 0 \tag{6.14}$$

or

$$(H - h_s)\left(\frac{\partial u}{\partial x} + \frac{\partial v}{\partial y}\right) - u\frac{\partial h_s}{\partial x} + v\frac{\partial H}{\partial y} = 0 \tag{6.15}$$

The momentum equations are as (6.3a,b):

$$\frac{du}{dt} = -g\frac{\partial}{\partial x}(h + h_s) + fv\,, \tag{6.16a}$$

$$\frac{dv}{dt} = -g\frac{\partial h}{\partial y} - fu\,, \tag{6.16b}$$

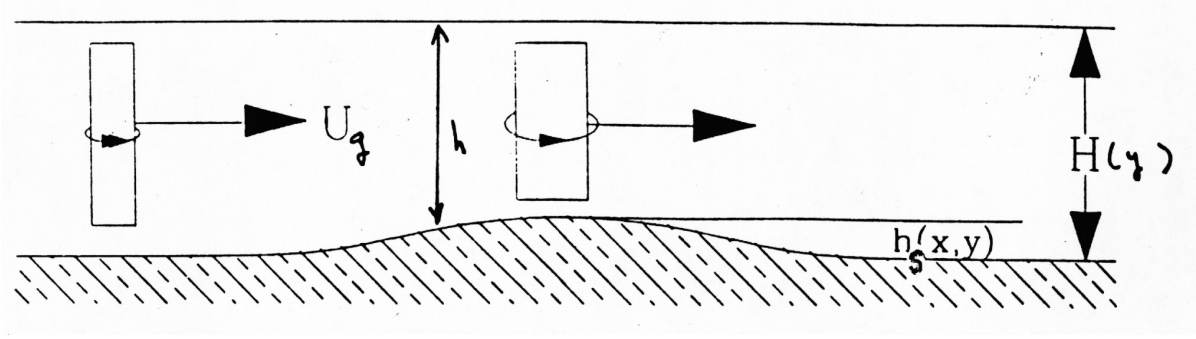

FIGURE 6.14. A model of flow over a mountain barrier (see the text for further explanation).

with

$$\frac{d}{dt} = \frac{\partial}{\partial t} + u\frac{\partial}{\partial x} + v\frac{\partial}{\partial y} \ . \tag{6.17}$$

From (6.16a,b) we derive an equation for the vertical component of the relative vorticity, $\zeta(=\partial v/\partial x - \partial u/\partial y)$. The result is

$$\frac{d\zeta}{dt} = -(f+\zeta)\left(\frac{\partial u}{\partial x} + \frac{\partial v}{\partial y}\right) - \beta v \ ,$$

where β=df/dy. To this equation we add a term on the r.h.s. $(=-r\zeta)$, which represents damping, where r is the damping rate coefficient (s^{-1}), as follows:

$$\frac{d\zeta}{dt} = -(f+\zeta)\left(\frac{\partial u}{\partial x} + \frac{\partial v}{\partial y}\right) - \beta v - r\zeta \ . \tag{6.18}$$

The reason for doing this will become apparent later in this section. The continuity equation (6.15) with

$$u_g = -\frac{g}{f_0}\frac{dH}{dy} \tag{6.19}$$

is

$$(H - h_s)\left(\frac{\partial u}{\partial x} + \frac{\partial v}{\partial y}\right) - u\frac{\partial h_s}{\partial x} - \frac{f_0 u_g}{g}v = 0 \ . \tag{6.20}$$

Now, assuming a **stationary state**, (6.18) with (6.20) becomes

$$u\frac{\partial \zeta}{\partial x} + v\frac{\partial \zeta}{\partial y} = -\frac{(f+\zeta)}{(H-h_s)}\left(u\frac{\partial h_s}{\partial x} + \frac{f_0 u_g}{g}v\right) - \beta v - r\zeta \ . \tag{6.21}$$

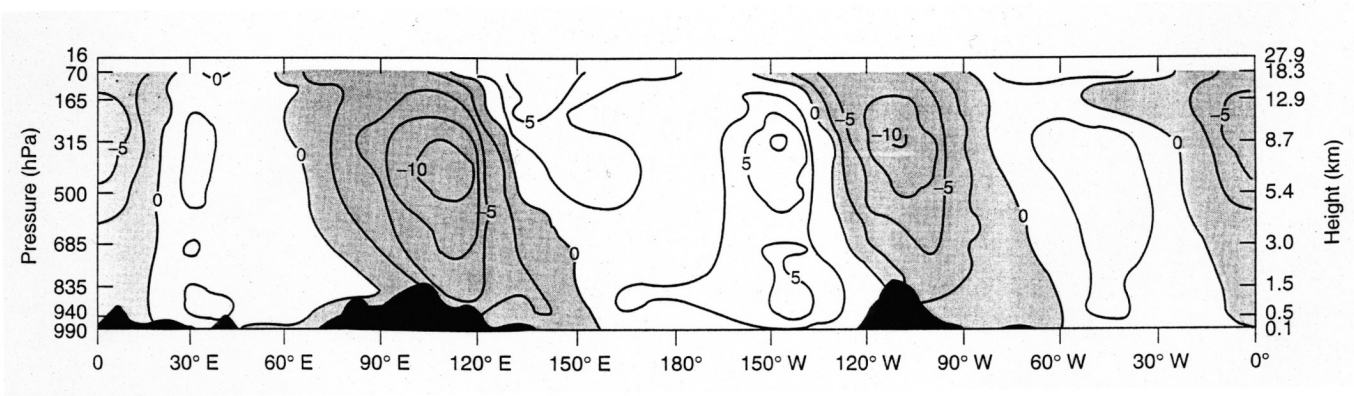

FIGURE 6.15. Observed stationary (time mean) planetary waves at 45° latitude in the northern hemisphere, in terms of the meridional component of the velocity (labeled in m/s), induced by mountains and other irregularities in the Earth's surface (S. Manabe and T.B. Terpstra, 1974: The effects of mountains on the general circulation of the atmosphere as identified by numerical experiments**. J.Atmos.Sci**., 31, 3-42).

To this equation we apply the **quasi-geostrophic approximation**[187], which in this case implies that $u \approx u_g$, $v \approx v_g$, $\zeta \approx \zeta_g = \partial v_g / \partial x$, $f = f_0 + \beta y \approx f_0$, $\zeta_g << f_0$, $h = H_0 + (dH/dy)y - h_s \approx H_0$ (implying that $h_s << H$) resulting in the following linear equation

$$\frac{d^2 v_g}{dx^2} + r\frac{dv_g}{dx} + \left(\frac{\beta}{u_g} + \frac{1}{a^2}\right) v_g = -\frac{f_0}{H_0}\frac{dh_s}{dx} \ , \tag{6.22}$$

where a is the Rossby radius of deformation (chapter 5), defined as

$$a \equiv \frac{\sqrt{gH_0}}{f_0} \ .$$

Suppose that

$$h_s(x) = h_0 \exp(ikx); \ v_g(x) = v_{g0} \exp(ikx); \ \zeta_g(x) = \zeta_{g0} \exp(ikx) \ , \tag{6.23}$$

so that

$$v_{g0} = -ik\zeta_{g0} \ , \tag{6.24}$$

then (6.22) yields

$$\zeta_{g0} = \frac{f_0 h_0}{H_0\left(\left(\frac{\beta}{u_g} + \frac{1}{a^2}\right) - k^2 + ikr\right)} \ . \tag{6.25}$$

From this we see that, if there is no damping (r=0), the relative vorticity is exactly in phase with the orography if

[187] The quasi-geostrophic approximation is explained in detail in chapter 9.

$$k^2 < \frac{\beta}{u_g} + \frac{1}{a^2} \ , \qquad (6.26a)$$

or exactly out of phase with the orography if

$$k^2 > \frac{\beta}{u_g} + \frac{1}{a^2} \ . \qquad (6.26b)$$

In other words, in theory, **troughs are observed in westerly flow over large scale mountain barriers, while ridges are observed in westerly flow over small scale mountain barriers.**

Eq. 6.25 also reveals that damping has the effect of introducing a phase shift between the orography and the wave. Explicit numerical solutions of (6.22) with realistic orography (for instance a single mountain barrier and not an infinite series of parallel ridges and valleys) and with r^{-1}= 5 days, show that the phase shift is such that the trough is located on the lee side of the mountain barrier, which is in accord with the observations (**figure 6.15**)[188]. The average wave pattern observed in the mean westerly flow is therefore identified as a stationary orographic Rossby wave, although it must be stated that thermal inhomogeneities in the zonal direction (i.e. differences in temperature and thermal inertia between continents and oceans) also explain at least part of the stationary wave pattern observed in **figure 6.15**.

Note, in **figure 6.15**, that the wave tilts backward with increasing height. This phase shift in the vertical direction is an important property of these waves, because it can be shown to be related to the meridional heat transport (chapter 11).

---

[188] For further reading see the following publications:

Charney, J.G. and A. Eliassen, 1949: A numerical method for predicting the perturbations of the middle latitude westerlies. **Tellus**, 1, 38-54.

Bolin, B., 1950: On the influence of the earth's orography on the general character of the westerlies. **Tellus**, 2, 184-195.

Held, I.M., 1983: Stationary and quasistationary eddies in the extratropical troposphere: theory. In **Large-scale dynamical processes in the atmosphere**. Edited by B.J. Hoskins and R.P. Pearce, Academic Press., p. 127-168.

Holton, J.R., 1993: The second Haurwitz Memorial Lecture: Stationary Planetary Waves. **Bull.Amer.Meteorol.Soc.**, 74, 1735-1742.

ABSTRACT OF CHAPTER 6

Chapter 6 is concerned with the interaction of hills, mountains and valleys with the motion of air in the atmosphere. Very diverse local wind systems are the result of this interaction. Well-known examples of such wind systems in Europe are **Foehn, Mistral and Bora** winds. The Bora can develop into a **downslope windstorm**, a non-linear effect which can be understood with the help of the relatively simple one-layer constant density "hydraulic model".

The fundamental parameter that governs the response of the air-flow over orography is the **Froude number**. There are several definitions of this parameter, but basically it represents the ratio of the large-scale background wind perpendicular to the mountain range or upstream of the valley to an intrinsic velocity that may be a phase velocity of waves (gravity or buoyancy waves) that are excited by the interaction of the basic flow with the orography.

The most important wind system that is related to orography is the **katabatic wind**, which is driven by cooling of air just above an inclined snow or ice surface, such as a glacier, or an ice cap. The wind regime over the huge ice caps of Greenland and Antarctica is dominated by the katabatic wind. Therefore, katabatic winds play an important role in climate because they largely determine the energy balance of these large ice caps and their rate of melt.

The response of air-flow around a mountain consists of phenomena such as **ship waves, vortex streets** and, on a larger scale, **lee-cyclones**.

The response to the largest mountain ranges, such as the Rocky-mountains, consists of **orographic Rossby waves**. The motion associated with these large scale stationary waves takes care of a large portion the heat flux from equator to poles.

Further reading

Books

Barry, R.G., 1992: **Mountain Weather and climate**. Routledge, 402 pp. (the best reference on "mountain meterology")

Holton, J.R., 2004: **An Introduction to Dynamic Meteorology (fourth edition)**. Academic Press, 535 pp. (chapters 5 and 9)

Markowski, P.M., and Y.P. Richardson, 2010: **Mesoscale Meteorology in Midlatitudes**. John Wiley, 430 pp. (chapters 12 and 13)

Articles

Gabersek, S., and D.R. Durran, 2004: Gap flows through idealized topography. Part 1: Forcing by large-scale winds in the nonrotating limit. **J.Atmos.Sci., 61**, 2846-2862.

Gross, B.D., 1994: Frontal interaction with isolated orography. **J.Atmos.Sci., 51**, 1480-

1496.

Holton, J.R., 1993: The second Haurwitz Memorial Lecture: Stationary Planetary Waves. **Bull.Amer.Meteorol.Soc.**, 74, 1735-1742.

Manabe, S., and T.B. Terpstra, 1974: The effects of mountains on the general circulation of the atmosphere as identified by numerical experiments**. J.Atmos.Sci**., 31, 3-42.

Pichler, H., R. Steinacker and A. Lanzinger, 1990: Cyclogenesis induced by the Alps. **Meteorol.Atmos.Phys., 43**, 21-29.

Smith, R.B., 1989: Hydrostatic flow over mountains. **Advances in Geophysics, 31**, 1-41.

List of problems (chapter 6)

This is the September 2014 edition of chapter 6 of the lecture notes on Atmospheric Dynamics., written by Aarnout van Delden (IMAU, Utrecht University, Netherlands, a.j.vandelden@uu.nl).

http://www.staff.science.uu.nl/~delde102/AtmosphericDynamics.htm